Graphical Abstract

Nanoscale dynamics in model phospholipid biomembranes probed by muon spin resonance spectroscopy: The effects of membrane composition and temperature on acyl chain and cholesterol motion

Iain McKenzie, Mitchell DiPasquale, Maksymilian Dziura, Thomas Gutberlet, Nathan Hartwig, Victoria L. Karner, Robert Scheuermann, Drew Marquardt

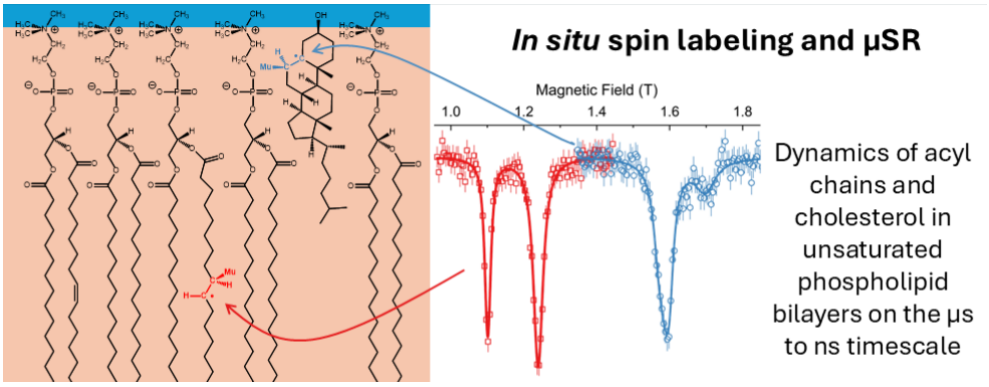

Highlights

Nanoscale dynamics in model phospholipid biomembranes probed by muon spin resonance spectroscopy: The effects of membrane composition and temperature on acyl chain and cholesterol motion

Iain McKenzie, Mitchell DiPasquale, Maksymilian Dziura, Thomas Gutberlet, Nathan Hartwig, Victoria L. Karner, Robert Scheuermann, Drew Marquardt

- Cholesterol causes stiffening of membranes composed of saturated (DPPC) and unsaturated lipids (POPC and DOPC)
- Muoniated radicals are used as local probes of dynamics at specific sites in phospholipid bilayers

Nanoscale dynamics in model phospholipid biomembranes probed by muon spin resonance spectroscopy: The effects of membrane composition and temperature on acyl chain and cholesterol motion

Iain McKenzie[a,b,c,*], Mitchell DiPasquale[d,1], Maksymilian Dziura[d], Thomas Gutberlet[e], Nathan Hartwig[a,c], Victoria L. Karner[a], Robert Scheuermann[f], Drew Marquardt[d,**]

[a] *Centre for Molecular and Materials Science, TRIUMF, 4004 Wesbrook Mall, Vancouver, V6T 2A3, BC, Canada*
[b] *Department of Chemistry, Simon Fraser University, 8888 University Drive, Burnaby, V5A 1S6, BC, Canada*
[c] *Department of Physics and Astronomy, University of Waterloo, 200 University Avenue West, Waterloo, N2L 3G1, ON, Canada*
[d] *Department of Chemistry and Biochemistry, University of Windsor, 401 Sunset Avenue, Windsor, N9B 3P4, ON, Canada*
[e] *Juelich Centre for Neutron Science, Forschungszentrum Juelich GmbH, Wilhelm-Johnen-Straße, Juelich, 52428, NRW, Germany*
[f] *Laboratory for Muon Spin Spectroscopy, Paul Scherrer Institute, Forschungsstrasse 111, Villigen, 5232, AG, Switzerland*

Abstract

The physical properties of lipid bilayers are known to depend on the composition, but there has recently been controversy about whether cholesterol (chol) does or does not stiffen biomembranes containing unsaturated phospholipids. Herein, avoided level crossing muon spin resonance (ALC-μSR) spectroscopy has been used to probe the local dynamics in model biomembranes composed of the saturated phospholipid 1,2-dipalmitoyl-sn-glycero-3-phosphocholine (DPPC), the unsaturated phospholipids 1-palmitoyl-2-oleoyl-glycero-3-phosphocholine (POPC) and 1,2-dioleoyl-sn-glycero-3-phosphocholine

*iain.mckenzie@triumf.ca
**drew.marquardt@uwindsor.ca
[1] Current address: Department of Physics and Astronomy, McMaster University, Hamilton, ON, Canada

(DOPC), and the sterol chol. The presence of chol significantly stiffens the acyl chains as evident from the reduction of the amplitude of restricted reorientational motion in the acyl chain at the C_9-C_{10} position and the increase of the torsional barrier for rotation about the bonds in the acyl chain. Swapping POPC for DOPC slightly increases the amplitude of restricted reorientational motion and decreases the torsional barrier of the acyl chains, but the magnitude of the effect is much smaller than the inclusion of chol.

Keywords: Phospholipid bilayer, Cholesterol, Membrane dynamics, Muon spin resonance, Spin label
PACS: 87.14.Cc, 76.75.+i
2000 MSC: 0000, 1111

---

1. Introduction

Phospholipids self assemble to form membranes that separate the contents of a cell from the outside and create compartments within the cell that have specific biological functions. The physical properties of the membrane, such as its fluidity, which allows embedded molecules and proteins to move within it, depend on the composition. Cholesterol (chol) is found in all animal cell membranes and is important for controlling membrane fluidity, organization, and other physicochemical parameters [1]. It is commonly assumed that chol stiffens membranes composed of saturated phospholipids but does not stiffen membranes made of unsaturated lipids, such as 1,2-dioleoyl-sn-glycero-3-phosphocholine (DOPC). However, a recent study using neutron spin-echo (NSE) spectroscopy, solid-state ^{2}H NMR spectroscopy, and molecular dynamics simulations found that chol causes local stiffening in DOPC membranes, which could indicate that a reassessment of existing concepts is necessary [2, 3] if not controversial [4].

The physical properties of the biomembrane are related to the motions of the individual components. Dynamic processes occurring in biomembranes are complex and the microscopic mechanisms are poorly understood [5]. The motions span a broad range of length and time scales. To better understand the behaviour of membranes it is necessary to probe the different dynamic processes of the constituents of the membrane. There are a variety of different analytical techniques used to study membrane dynamics, with each being sensitive to different ranges of length and time scales. Neutron scattering is a powerful technique for probing dynamics but is averaged over the

sample [6]. One can probe the local environment and dynamics of specific components in the membrane by spin labelling. This could be with stable isotopes such as deuterium and characterizing the molecules with NMR [7] or stable radicals such as nitroxides and characterizing the spin probes with EPR [8]. Muoniated radicals can be used to spin label specific components in soft matter [9]. Muoniated radicals are formed by the addition of muonium (Mu), which behaves chemically like a light isotope of hydrogen, to unsaturated bonds. These in situ generated spin probes are characterized by a magnetic resonance technique called avoided level crossing muon spin resonance (ALC-μSR) spectroscopy. ALC-μSR is sensitive to motion on timescales ($\sim 10^{-6} - 10^{-9}$ s) intermediate to that accessible by NMR and neutron scattering [6] and the transient spin probes are considerably less perturbing than the nitroxide radicals used in EPR and fluorescent probes [10]. The muoniated spin probes are effectively in the infinitely dilute limit as only a few radicals are present in a volume of a few mL at any moment.

We have used ALC-μSR to characterize muoniated spin labels introduced into model phospholipid biomembranes. There were previous μSR studies of the phospholipid DOPC (1,2-dioleoyl-sn-glycero-3-phosphocholine) in the solid state [11], cholesterol (chol) in the solid state [12], and a liposome composed of a 1:1 mixture of 1,2-dipalmitoyl-sn-glycero-3-phosphocholine (DPPC) and chol [12] using the longitudinal field repolarization method [9]. This method is not useful for accurately measuring the hyperfine parameters of muoniated radicals and did not provide any relevant information about dynamics in the membrane. ALC-μSR is a significantly more sensitive method for characterizing muoniated radicals and we contend this is the first direct observation of muoniated spin probes within phospholipid membranes. We have been aiming to determine how the composition of the membrane affects the local dynamics as sensed by the spin probe at specific locations within the biomembranes. We examined five biomembranes composed of various combinations of DPPC, DOPC, chol and 1-palmitoyl-2-oleoyl-glycero-3-phosphocholine (POPC): 2:1 DPPC:POPC, 2:1 DPPC:DOPC, 2:1:1 DPPC:POPC:chol, 2:1:1 DPPC:DOPC:chol, and 73:27 DPPC:chol. The structures of the phospholipids and chol are shown in Figure 1.

We have found that swapping POPC for DOPC has little effect on the dynamics at the C_9-C_{10} position of the acyl chains while including chol in the biomembrane dramatically slows the dynamics and restricts the motions of the acyl chains. This supports the finding that chol can stiffen membranes

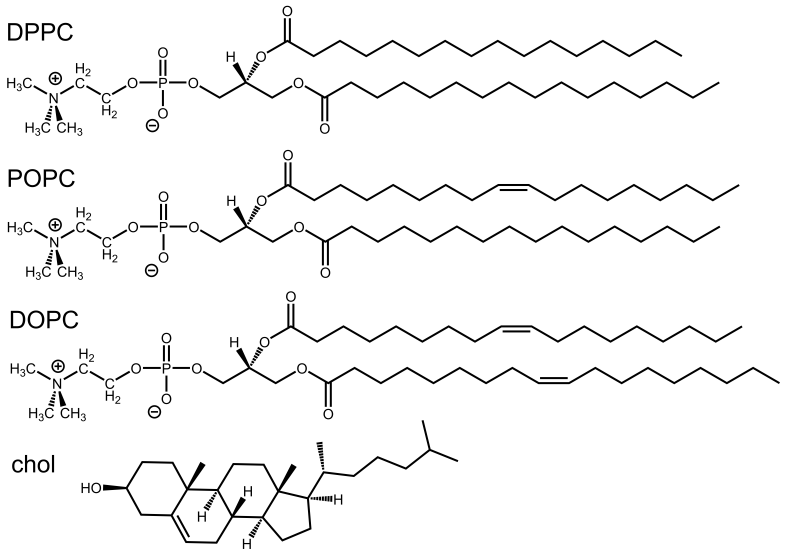

Figure 1: Structures of DPPC, POPC, DOPC, and chol.

made of unsaturated lipids.

2. Experimental

The synthetic lipids DPPC, DPPG, POPC, and DOPC were purchased from Avanti Polar Lipids (Alabaster, AL). Cholesterol was purchased from Sigma-Aldrich (Oakville, ON). All water used was from a Milli-Q Direct Water Purification System in order to ensure ultrapure water with a resistivity of 18.2 MΩ·cm. Prior to use, the water was degassed by sonication in vacuo at 50 °C for 30 minutes. Vacuum was broken by argon purge and the water was stored in an airtight container with little headspace only briefly before use.

All samples were created with extreme precaution to ensure samples were not exposed to oxygen during the preparation. The presence of molecular oxygen can affect Mu addition and lead to quenching of the spectra. For this reason, the majority of the preparation was conducted in a glovebox purged with argon gas with oxygen levels monitored by an oxygen detector. All samples were made from the same lipid stock solutions in chloroform. Note, all samples were doped with the negatively charged DPPG to ensure unilamellarity [13]. Stoichiometric mixtures of lipids were combined as chloroform stocks, then solvent was evaporated in vacuo for at least 12 h to

form a thin lipid film. To remove the samples from the vacuum oven, the chamber was purged and blanketed with argon. Inside the glovebox, samples were hydrated to a concentration of 20 mg/mL using freshly degassed water. Samples were sealed inside the box with a headspace of argon prior to five freeze-thaw-vortex cycles -80 and 60 °C. Multilamellar vesicles were extruded to unilamellar vesicles (ULV) by 31 passes through a hand-held mini-extruder (Avanti Polar Lipids) equipped with an 100 nm pre-diameter polycarbonate filter. ULV were studied so that rotation of vesicles was slow enough to not contribute to broadening of the ALC resonances as has been previously observed in $C_{12}E_4$ micelles [14]. The extruders were assembled on the bench-top but were purged with degassed water and loaded with sample inside the glove box to create an airtight seal. The efficiency of the extrusion was determined with dynamic light scattering using a Malvern ZetaSizer Nano ZS (Malvern Panalytical, Malvern, UK). In the glovebox, completed samples were dispensed into aluminum sample cells with 50 μm thick titanium foil windows, allowing for no headspace before being sealed by Teflon plugs and cyanoacrylate glue, which did not come into contact with the solution.

ALC-μSR measurements were performed using the HELIOS spectrometer on the M15 beamline at TRIUMF. There is a significant non-linear background due to changes in the beam spot and positron spiraling in the applied magnetic field. It is very sensitive to the size, density, and position of the sample in the spectrometer, and is affected by temperature. The non-linear background makes it difficult to measure broad resonances where the width is comparable to the curvature of the background. Raw data were corrected for the field dependent background by subtracting a polynomial from the experimental data. Least square fitting of multiple Lorentzians was applied to the corrected data using a procedure based on the Minuit function minimization library, and the fits to the background corrected and raw data were visually compared in addition to obtaining an acceptable minimized χ^2 value for the least squares fit.

DFT calculations were performed with Gaussian 09 [15] using the unrestricted B3LYP density functional. The 6-311G*(d,p) basis set was used for calculations on a fragment of the acyl chains and the 6-31g(d,p) basis set was used for calculations of chol with a methyl group replacing the hydrocarbon tail. Muonium was treated as an isotope of H with a magnetic moment of 8.890597 μ_N. The light mass of the muon was mimicked by increasing the C-Mu bond length by a factor of 1.076 from its optimized value, fixing it, and partially optimizing the rest of the radical. The empirical factor is based

on the quantum calculations of Böhm et al. for the muoniated ethyl radical [16].

3. Methodology

The ALC-μSR technique has been extensively reviewed [9], so only a brief summary is given here. The technique involves measuring the time-integrated asymmetry as a function of the applied magnetic field. Resonances, which correspond to a loss of muon spin polarization, occur when spin states are mixed through the isotropic or anisotropic components of the hyperfine interaction. We typically observe two types of resonances, which are characterized by the selection rule $\Delta M = 0$ and ± 1, where M is the sum of the m_z quantum numbers of the muon, electron, and nuclear spins. The resonances are referred to as Δ_0 and Δ_1 resonances, respectively.

The Δ_0 resonance field depends on both the isotropic muon hyperfine coupling constant (hfcc), A_μ, and the isotropic proton hfcc, A_p, and is given by:

$$B_\mathrm{res}^{\Delta_0} = \frac{1}{2}\left[\frac{A_\mu - A_\mathrm{p}}{\gamma_\mu - \gamma_\mathrm{p}} - \frac{A_\mu + A_\mathrm{p}}{\gamma_\mathrm{e}}\right], \tag{1}$$

where γ_μ, γ_p and γ_e are the muon, proton, and electron gyromagnetic ratios, respectively. There can also be Δ_0 resonances from other nuclei with non-zero spins such as ^{14}N and ^{13}C. In fact, there are as many Δ_0 resonances as there are nuclei with non-zero spin in the radical, but in practice we focus on protons that have large hfccs as these result in the large Δ_0 resonances. This is due to the limited amount of beam time available. The isotropic hfccs provide information about the structure and conformation of the muoniated spin probe.

Δ_1 resonances are only observed when radicals are undergoing anisotropic motion where the muon dipolar hyperfine interaction is not completely averaged. In the present context, the mere presence of a Δ_1 resonance is taken as a sensitive indicator of small anisotropy of the radical reorientational motion on a time scale of typically 50 ns. The Δ_1 resonance field is given by:

$$B_\mathrm{res}^{\Delta_1} = \frac{1}{2}\left[\frac{A_\mu}{\gamma_\mu} - \frac{A_\mu}{\gamma_\mathrm{e}}\right], \tag{2}$$

The muon dipolar hyperfine interaction can be described as a tensor with three principal components. Rapid rotation about an axis generates an axially symmetric dipolar hyperfine tensor. It can be described in terms of the

parallel muon dipolar hfcc ($D_\mu^{\parallel}$) and the perpendicular muon dipolar hfcc ($D_\mu^{\perp}$). Wobbling of the rotation axis will further average the dipolar coupling. We denote this by the use of angled brackets and refer to this as the motionally-averaged muon dipolar hyperfine coupling constant ($\left\langle D_\mu^{\parallel} \right\rangle$). We assume that the rotation axis wobbles randomly within a cone of half-angle θ_{C} (restricted random walk model) [17]. The vibrationally-averaged muon dipolar coupling constant becomes:

$$\left\langle D_\mu^{\parallel} \right\rangle = D_\mu^{\parallel} \left(\frac{\cos\theta_{\mathrm{C}} + \cos^2\theta_{\mathrm{C}}}{2} \right) \tag{3}$$

The total change of the time-integrated muon polarization as a function of applied magnetic field due to a Δ_1 resonance is given by:

$$\Delta \bar{P}_z^{\Delta_1}(B,\theta) = \int_0^{\infty} \frac{(4h_{\mathrm{R}}/N)(\nu_r^{\Delta_1})^2}{(\lambda/2\pi)^2 + (\nu_r^{\Delta_1})^2 + \gamma_\mu^2 (B - B_{\mathrm{res}}^{\Delta_1})^2} \sin\theta d\theta \tag{4}$$

h_{R} is the fraction of muons forming the muoniated radical, N is the dimension of the Pauli spin operator matrix, which depends on the number of spins with $I > 0$ in the radical, λ is the on-resonance damping rate, and θ is the angle between the unique axis of the axial dipolar tensor and the magnetic field. The frequency on resonance ($\nu_r^{\Delta_1}$) is

$$\nu_r^{\Delta_1} = \frac{3}{4} \left\langle D_\mu^{\parallel} \right\rangle \sin\theta\cos\theta \tag{5}$$

If the Δ_1 resonance has an asymmetric lineshape, $\left\langle D_\mu^{\parallel} \right\rangle$ can be determined by fitting the resonance with the preceding two expressions derived by Roduner [18]. If the Δ_1 resonance has a Lorentzian-like lineshape, we have recently shown the magnitude of $\left\langle D_\mu^{\parallel} \right\rangle$ can be determined if a Δ_0 resonance is also observed. $\left\langle D_\mu^{\parallel} \right\rangle$ is obtained from the Δ_1 amplitude (A_1), Δ_1 width (Γ_1), muon hfcc, Δ_0 amplitude (A_0), Δ_0 width (Γ_0), and proton hfcc [19].

$$|\left\langle D_\mu^{\parallel} \right\rangle| \approx c_1 \cdot x + c_2 \cdot x^2 + c_3 \cdot x^3 \tag{6}$$

where $c_1 = 1.114(1) \times 10^{-2}$ MHz^{-1}, $c_2 = 6.5(22) \times 10^{-6}$ MHz^{-2}, $c_3 = 3.1(8) \times 10^{-8}$ MHz^{-3}, and

$$x = \frac{A_\mu A_{\mathrm{p}}}{(A_\mu - A_{\mathrm{p}})} \sqrt{\frac{A_1\Gamma_1}{[A_0/c^2]\,\Gamma_0}} \tag{7}$$

c has a value of $\sqrt{n}$ where n is the number of protons contributing to the Δ_0 resonance.

Since we measure $|\left\langle D_\mu^\parallel \right\rangle|$, we can determine θ_C if $D_\mu^\parallel$, the value for pure uniaxial rotation, is known. We cannot measure $D_\mu^\parallel$, so we estimate it using DFT calculations and the method described by Weil and Bolton [20]:

$$D_\mu^\parallel = \left[\mathbf{n}^T \cdot \mathbf{A} \cdot \mathbf{A}^T \cdot \mathbf{n}\right]^{1/2} - A_\mu \tag{8}$$

where $\mathbf{n}$ is the rotation axis, $\mathbf{n}^T$ is its transpose, $\mathbf{A}$ is the hyperfine tensor, and $\mathbf{A}^T$ is its transpose. The rotation axis is transformed from the molecular coordinate system to the coordinate system of the muon hyperfine tensor.

4. Results and discussion

4.1. Muoniated Radicals and Assignment of ALC-μSR Spectra

ALC-μSR spectra of 2:1 DPPC:POPC, 2:1:1 DPPC:POPC:chol, and 73:27 DPPC:chol ULVs at 40 °C are shown in Figure 2. There are two resonances in the 2:1 DPPC:POPC spectrum at 1.1142(5) and 1.2538(6) T, three resonances in the ALC-μSR spectrum of 2:1:1 DPPC:POPC:chol at 1.145(2), 1.284(3) T, and 1.591(3) T, and a single resonance at 1.596(3) T in the ALC-μSR spectrum of 73:27 DPPC:chol.

The first step is to assign the resonances. The resonances are due to muoniated radicals that are produced by Mu addition to the C=C bonds of POPC, DOPC, and chol. The dilute nature of Mu means that only one muoniated radical will be produced by reaction with DOPC. Mu addition to C=O and P=O bonds is much slower than addition to C=C bonds and so does not result in the generation of spin probes at those sites [9].

The Lorentzian resonances at ∼1.12 and ∼1.26 T are present only in the samples containing POPC, so they must be due to the Mu adducts of POPC. The assignment of these resonances is made in part based on the similarity of the measured hyperfine parameters with those of the Mu-sec-butyl radical, which is formed by Mu addition to either cis-2-butene or trans-2-butene [21]. In the case of POPC, we cannot distinguish between Mu addition at carbons 9 and 10. The resulting radicals are both alkyl radicals in the middle of a long chain thus making their contributions to the signal indistinguishable. The structures of the radicals are shown in Figure 3 and are referred to as Mu_9-POPC and Mu_{10}-POPC, respectively. We will collectively refer to these radicals as the Mu adducts of POPC. These radicals have structures very

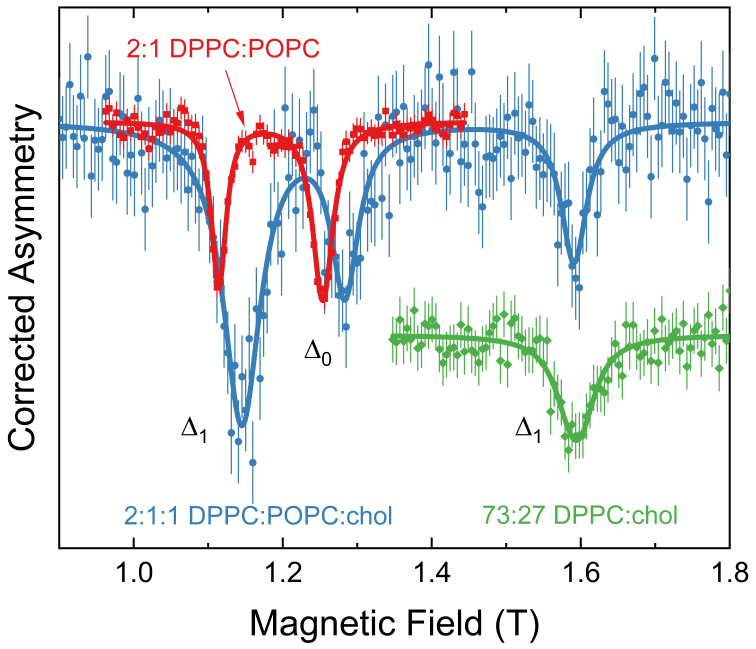

Figure 2: Background-subtracted ALC-μSR spectra of the 2:1 DPPC:POPC, 2:1:1 DPPC:POPC:chol, and 73:27 DPPC:chol unilamellar vesicles at 40 °C. The spectrum of 2:1 DPPC:POPC has been scaled by a factor of 0.363 so the amplitude of the Δ_0 resonance is the same as in the 2:1:1 DPPC:POPC:chol spectrum. The 73:27 DPPC:chol spectrum has been offset vertically for clarity.

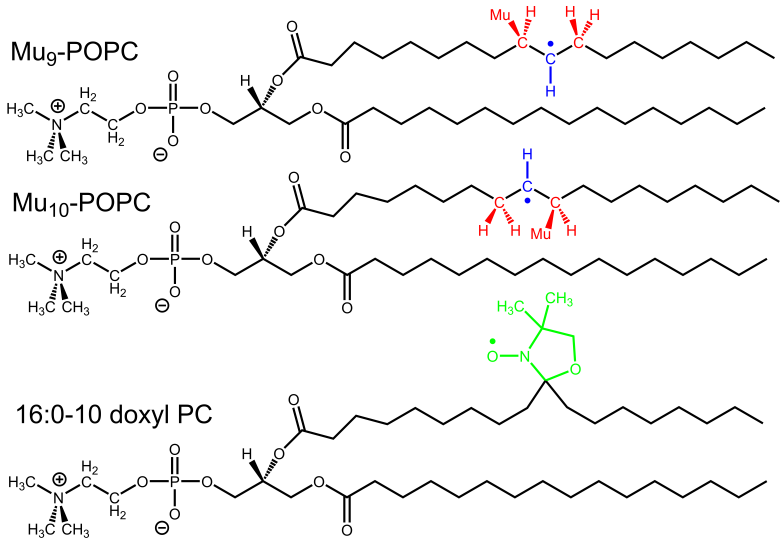

Figure 3: Structures of the Mu adducts of POPC and a stable nitroxide spin probe, 1-palmitoyl-2-stearoyl-(10-doxyl)-sn-glycero-3-phosphocholine (16:0-10 doxyl PC). The radical centres of the muoniated radicals are shown in blue while the β nuclei (adjacent to the radical centres) are shown in red. The Mu adducts of DOPC have similar structures except that there is a double bond in the other chain. The stable nitroxide substituent of 16:0-10 doxyl PC is highlighted in green.

similar to DPPC, with the only difference being they are missing an H, and are much smaller perturbations than the bulky, commonly used nitroxide spin probes. The peak at 1.12 T is the Δ_1 resonance of the Mu adducts of POPC and A_μ is 303.49(15) MHz in 2:1 DPPC:POPC and 311.9(5) MHz in 2:1:1 DPPC:POPC:chol. The peak at ∼1.26 T is a Δ_0 resonance due to hyperfine coupling with the β proton of the CHMu group and the two β protons of the CH_2 group on the opposite side of the radical centre. A_p is 69.15(14) MHz in 2:1 DPPC:POPC and 72.0(5) MHz in 2:1:1 DPPC:POPC:chol. The hyperfine parameters of the muoniated spin probes depend strongly on the conformation of the acyl chain and are larger in the biomembranes containing chol.

The resonances at ∼1.59 T are present only in the samples containing chol, so we can conclude that they are due to a muoniated radical formed by Mu addition to chol. The assignment was made by comparing the ALC-μSR spectrum with that of the chiral nematic liquid crystal cholesteryl nonanoate [22]. The observed radical was formed by Mu addition to the secondary

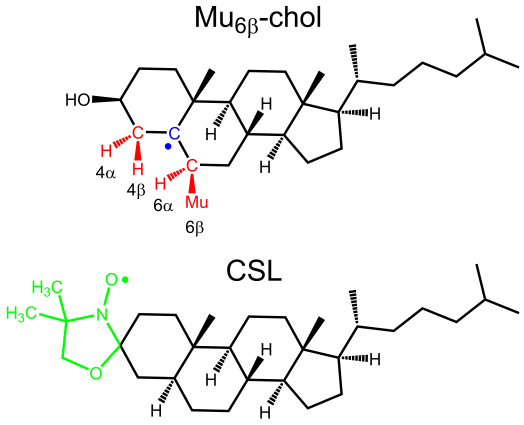

Figure 4: Structure of the observed Mu adduct of chol (Mu-6β-chol) and 3β-doxyl-5α-cholestane, the cholestane spin label (CSL). The radical centre of the muoniated radical is shown in blue while the β nuclei (adjacent to the radical centres) are shown in red. The stable nitroxide substituent of CSL is highlighted in green.

carbon of the C=C bond from the so-called "rough" or β face. We refer to this as the Mu-6β-chol radical based on the position of Mu, and its structure is shown in Figure 4. The muoniated radical is a much smaller perturbation than commonly used nitroxide radicals such as 3β-doxyl-5α-cholestane. The peak at $\sim$1.59 T is a Δ_1 resonance and the corresponding A_μ values are 434.7(8) MHz in 73:27 DPPC:chol and 433.4(8) MHz in 2:1:1 DPPC:POPC:chol. Addition of Mu from the "smooth" or α face results in a radical with a much smaller A_μ value and this was not observed.

4.2. Temperature and Composition Dependence of Acyl Chain Dynamics

The size, shape, and position of the Lorentzian-like ALC resonances and their variation with temperature can provide information about the dynamics of the acyl chains in the model biomembranes at the C_9-C_{10} position. We investigated how the dynamics of the acyl chains depends on composition, with measurements looking at the effect of swapping POPC for DOPC and the inclusion of chol. ALC-μSR spectra over a range of temperatures are shown in Figure 5.

The spectra of 2:1 DPPC:POPC and 2:1 DPPC:DOPC at 35 °C and above are nearly identical. The Δ_1 and Δ_0 resonances in both samples shift to higher magnetic fields with decreasing temperature and broaden. Where the spectra differ is below 35 °C where there is an additional broad resonance

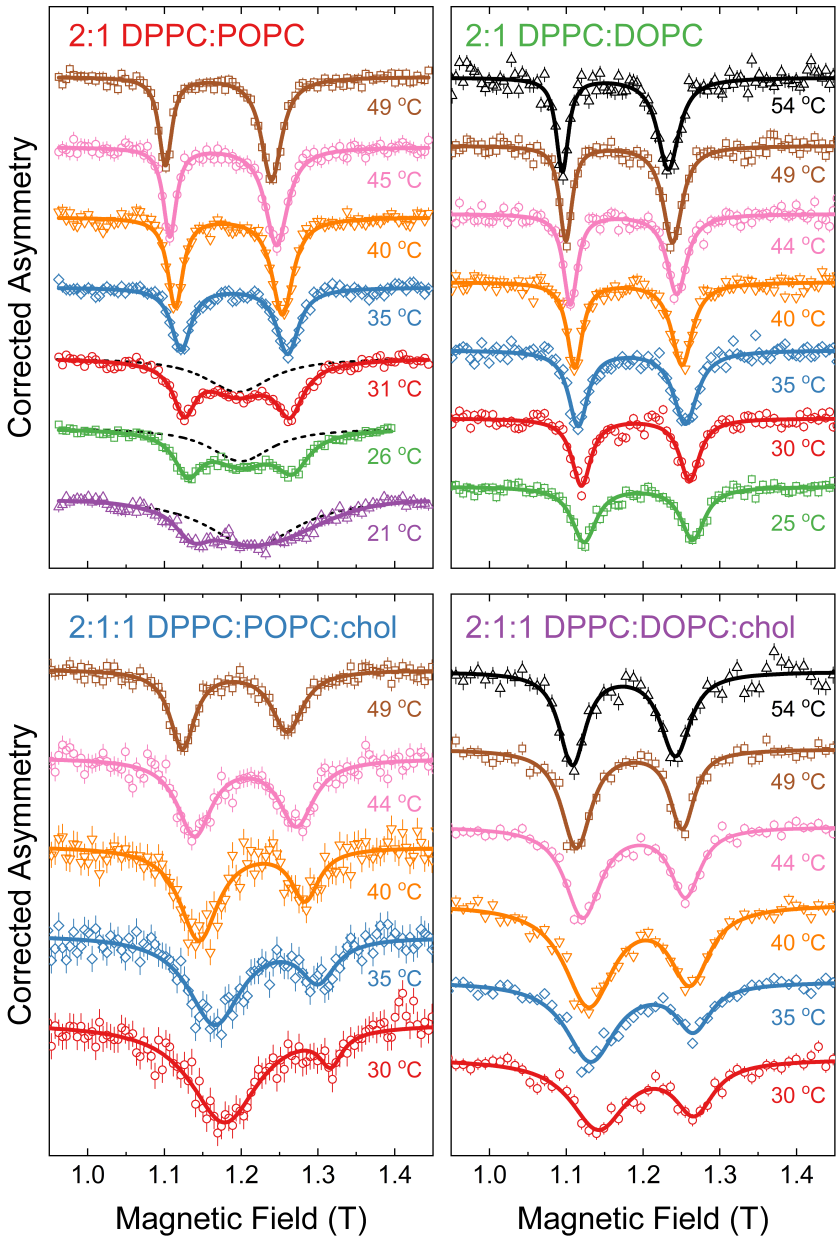

Figure 5: Background-subtracted ALC-μSR spectra of 2:1 DPPC:POPC, 2:1 DPPC:DOPC, 2:1:1 DPPC:POPC:chol, and 2:1:1 DPPC:DOPC:chol unilamellar vesicles as a function of temperature. The spectra are offset vertically for clarity. The dashed lines in the 2:1 DPPC:POPC spectra are the broad feature observed at 21 to 31 °C.

in 2:1 DPPC:POPC. This is due to coexistence between L_α and L_β phases of DPPC:POPC bilayers [23]. The relatively narrow Δ_1 and Δ_0 resonances are due to muoniated spin probes in the L_α phase and the broad feature is due to muoniated spin probes in the L_β phase where the acyl chains are frozen. The broad feature is difficult to disentangle from the non-linear background. The amplitude of the Δ_0 resonance associated with the L_α phase, which is related to how much of the muoniated radical is formed, decreases with decreasing temperature and has almost disappeared at 21 °C. This is because the volume fraction of the L_α domains decrease with decreasing temperature in this coexistence region. In 75:25 DPPC:POPC, which is close to the composition studied here, coexistence is thought to occur below ∼40 °C [23]. By 32 °C, the domains are no longer compact and the system is near the percolation point of the lattice (50%). The liquid domains disappear around 15-20 °C. Coexistence between the L_α and L_β phases is not observed at either 35 or 40 °C. This could either be due to the sample being completely in the L_α phase or there could be preferential partitioning of the muoniated spin probe from the L_β phase to the L_α at these temperatures. This would be possible, regardless of where the parent POPC was located when the muoniated probe was formed, because the muoniated spin probes can move a substantial distance during their lifetime of several μs. The lateral diffusion rate of DPPC is 17.8 $\mu m^2/s$ at 45 °C [24], which corresponds to a displacement due to 2D Brownian motion of ∼8 nm in 1 μs. We suggest that the lateral diffusion rate of the muoniated spin probes will be of similar magnitude. No broad resonance was observed in 2:1 DPPC:DOPC at low temperatures, which could indicate no coexistence of liquid and gel domains.

The amplitude of the Δ_0 resonance in 2:1:1 DPPC:POPC:chol is significantly smaller than the corresponding resonance in 2:1 DPPC:POPC as the muon polarization is spread out over more types of muoniated radical. As is evident from Figure 2, the resonance fields of the Mu adducts of POPC, and consequently the hfccs, have larger values than in the 2:1 DPPC:POPC biomembrane. It is also evident from just a visual inspection of the spectra that Δ_1 resonance is also significantly larger relative to the Δ_0 resonance in the presence of chol than in the 2:1 DPPC:POPC biomembrane. This indicates that the motion of the muoniated spin probes, and by inference the acyl chains, is more restricted in the presence of chol. The relative amplitude of the Δ_1 resonance to the Δ_0 resonance and the positive shift of the resonances compared with the chol-free membrane is less than in the 2:1:1 DPPC:POPC:chol membrane.

Membrane components of different nature and interface show non-ideal mixing behavior leading to phenomena such as domain formation [25, 26]. The formation of raft-like liquid ordered (L_o) domains in model membrane systems has been investigated to great extent using confocal fluorescence microscopy [27], calorimetry [28], NMR [29], quasi-elastic neutron scattering (QENS) and small angle neutron scattering (SANS) [30, 31, 32, 33, 34], and EPR [35]. The L_o domains in 2:2:1 DPPC:POPC:chol are $\sim$7 nm across at 35 °C [34]. Based on the lateral diffusion rates discussed above and the size of the domains, it is likely that the muoniated spin probes could partition into the POPC rich regions, even if they are formed in the POPC deficient and chol rich rafts.

The magnitude and temperature dependence of the muon hfccs provide information about the average conformation of the acyl chain about the radical centre. The muon hfcc depends dramatically on the conformation of the acyl chain. The observed muon hfcc is a Botltzmann-weighted average over the various torsional states and can be affected by intermolecular interactions with surrounding molecules. The muon hfccs were determined using Eq. 1 and the values as a function of temperature are shown in Figure 6. The motionally-averaged dipolar muon hfccs provide information about the amplitude of restricted motion of the acyl chain. $|\left\langle D_\mu^{\parallel} \right\rangle|$ was determined using Eq. 4 and 5 and the values as a function of temperature are shown in Figure 7.

We have performed DFT calculations on a simplified system, the Mu-sec-butyl radical [21], which is a four-carbon-long fragment of the acyl chain (Figure 8), in order to interpret the results described above. DFT calculations were performed as a function of the dihedral angle around C_α-C_βHMu (ϕ). This contrasts with a previous report of DFT calculations of the Mu-sec-butyl radical where calculations were only made at a limited number of configurations [36]. The structure was partially optimized as a function of this angle, and then, to account for vibrational averaging and the light mass of Mu, the C-Mu bond has been intentionally elongated to 1.076 times the corresponding equilibrium C-H bond length, and the structure was partially reoptimized with the additional constraint. The calculated angular variation of the energy and hyperfine parameters are shown in Figure 9. The angular dependence of the hyperfine parameters is due to changes in the overlap of the C-Mu bond with the orbital containing the unpaired electron and can be approximated by the McConnel equation.

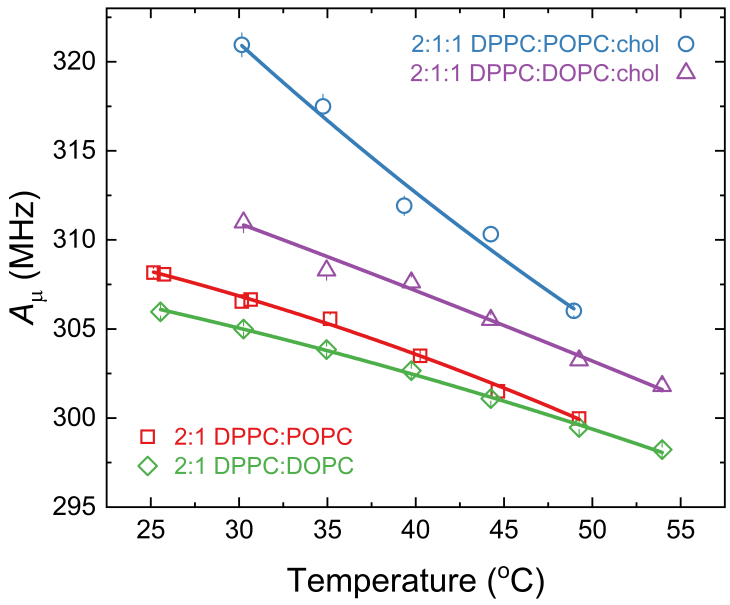

Figure 6: Temperature dependence of the isotropic muon hfcc of the Mu adducts of POPC in unilamellar vesicles of 2:1 DPPC:POPC and 2:1:1 DPPC:POPC:chol and the Mu adducts of DOPC in unilamellar vesicles of 2:1 DPPC:DOPC and 2:1:1 DPPC:DOPC:chol.

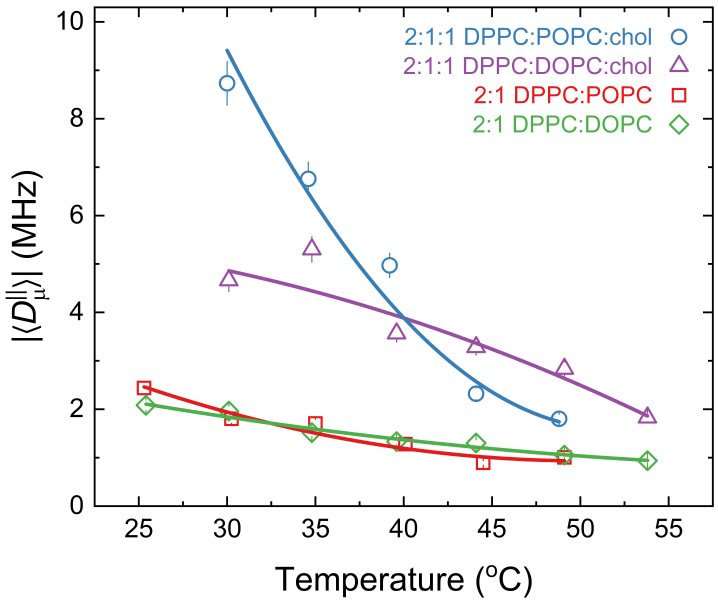

Figure 7: Temperature dependence of the motionally averaged dipolar muon hfcc of the Mu adducts of POPC in unilamellar vesicles of 2:1 DPPC:POPC and 2:1:1 DPPC:POPC:chol and the Mu adducts of DOPC in unilamellar vesicles of 2:1 DPPC:DOPC and 2:1:1 DPPC:DOPC:chol. The solid lines are a guide for the eyes.

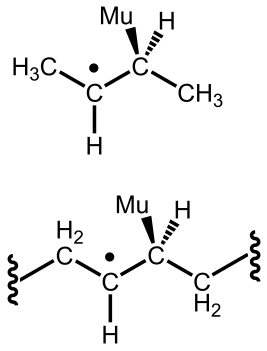

Figure 8: Structure of the Mu-sec-butyl radical and a fragment of the Mu adducts of POPC and DOPC.

The calculated torsional barrier for the Mu-sec-butyl radical is 8.1 kJ mol^{-1}. We have assumed that the thermally averaged value for a parameter 'X' is given by the Boltzmann factor.

$$X = \frac{\sum X(\phi) e^{-\Delta E(\phi)/k_{\mathrm{B}}T}}{\sum e^{-\Delta E(\phi)/k_{\mathrm{B}}T}} \tag{9}$$

The torsional potential means that the radical was undergoing very large amplitude torsional motion around $\phi \sim 180°$. Our simulation for the Mu-sec-butyl radical matches the experimental data of A_μ in the liquid state (-103 to -23 °C) if we include an additional factor of 1.136 in the muon hyperfine coupling constant (Figure 10).

The torsional potential of the Mu-sec-butyl radical cannot account for the temperature dependence of A_μ in the samples with or without chol (Figure 9). We have assumed that the torsional potential of the Mu adducts of POPC and DOPC will have a similar angular dependence to the Mu-sec-butyl radical, but the barrier height will be different due to the longer chains and their interactions with neighbouring chains exerting constraints on torsional motion. This can be approximated by multiplying the torsional potential shown in Figure 9 by a constant factor. The torsional barrier can be seen as a proxy for the stiffness of the acyl chains. Good agreement with the experimental data for the model biomembranes can be achieved if we assume that the torsional barrier depends on temperature and composition of the membrane. The barrier heights that reproduce the experimental data are given in Figure 11. In all samples the barrier decreases with increasing temperature and are consistent with a decrease in chain packing. The torsional barrier is larger in the presence of chol which indicates more of a trans conformation and is consistent with NMR studies [37]. Swapping DOPC for POPC leads to a reduction in the torsional barrier, indicating a softening of the membrane, but the effect is smaller compared with including chol.

$D_\mu^{\parallel}$, the value for pure uniaxial rotation, was calculated as a function of dihedral angle for motion about the lowest moment of intertia using Eq. 6 (Figure 9). The torsional barriers shown in Figure 11 along with Eq. 7 were used to calculate the expected value of $D_\mu^{\parallel}$ in each sample as a function of temperature. We then used Eq. 3 to estimate θ_{C} based on the measured $|\left\langle D_\mu^{\parallel} \right\rangle|$ values (Figure 12).

There is very little difference in θ_{C} between 2:1 DPPC:POPC and 2:1 DPPC:DOPC. In 2:1 DPPC:POPC, θ_{C} increases from 60° at 25 °C to 77°

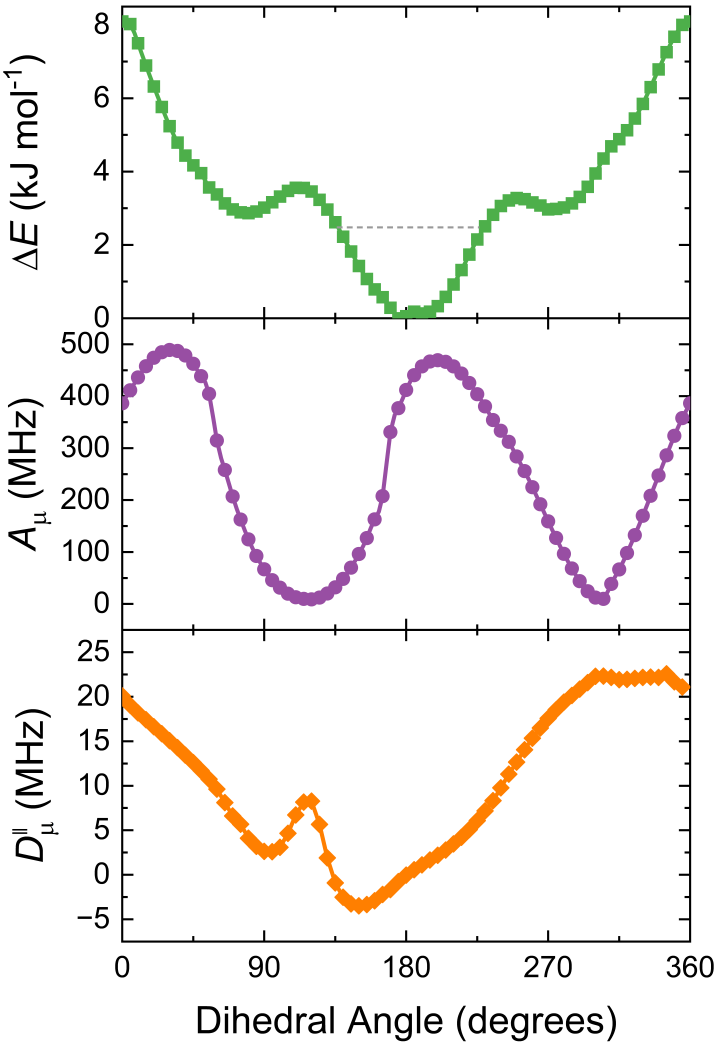

Figure 9: Dependence of the relative energy (ΔE), the isotropic muon hfcc (A_μ), and the muon dipolar hfcc for rapid uniaxial rotation about the axis with the smallest moment of inertia ($D_\mu^{\parallel}$) of the Mu-sec-butyl radical on the dihedral angle. UB3LYP/6-311G*(d,p). The dotted horizontal line corresponds to $k_\mathrm{B}T$ at 25 °C.

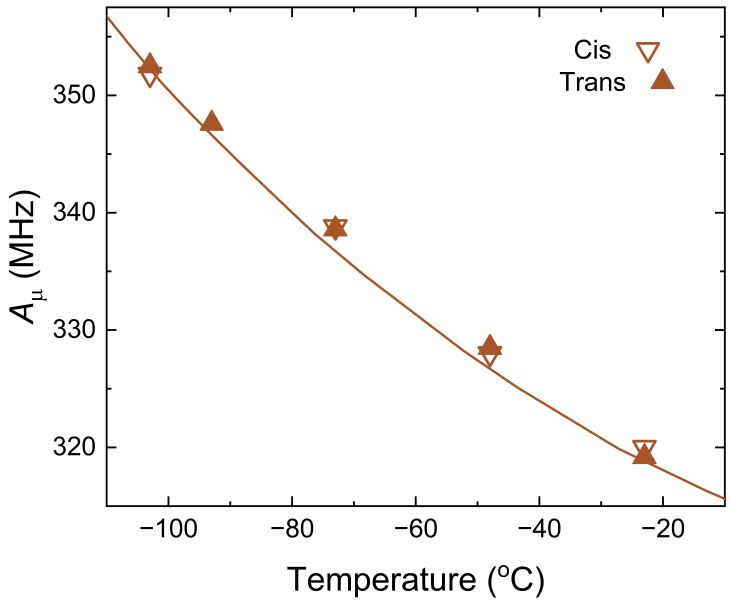

Figure 10: Temperature dependence of the isotropic muon hfcc of the Mu-sec-butyl radical in the liquid phases of cis-2-butene and trans-2-butene [21]. The solid line is based on the values reported in Figure 9 with Eq. 7 and an additional factor of 1.136 for the muon hfcc.

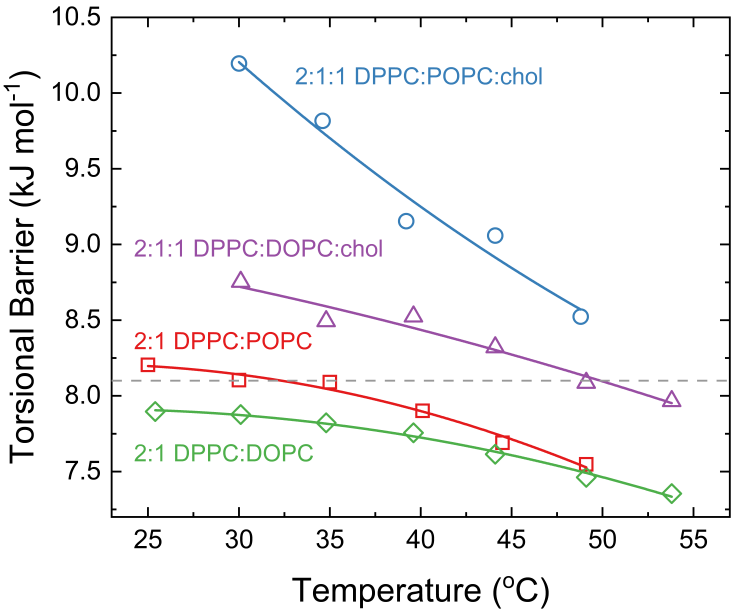

Figure 11: Temperature dependence of the torsional barrier for the Mu adducts of POPC in 2:1 DPPC:POPC and 2:1:1 DPPC:POPC:chol unilamellar vesicles and the Mu adducts of DOPC in 2:1 DPPC:DOPC and 2:1:1 DPPC:DOPC:chol unilamellar vesicles based on the isotropic muon hyperfine coupling constants. The horizontal dashed line is the calculated barrier for the Mu-sec-butyl radical.

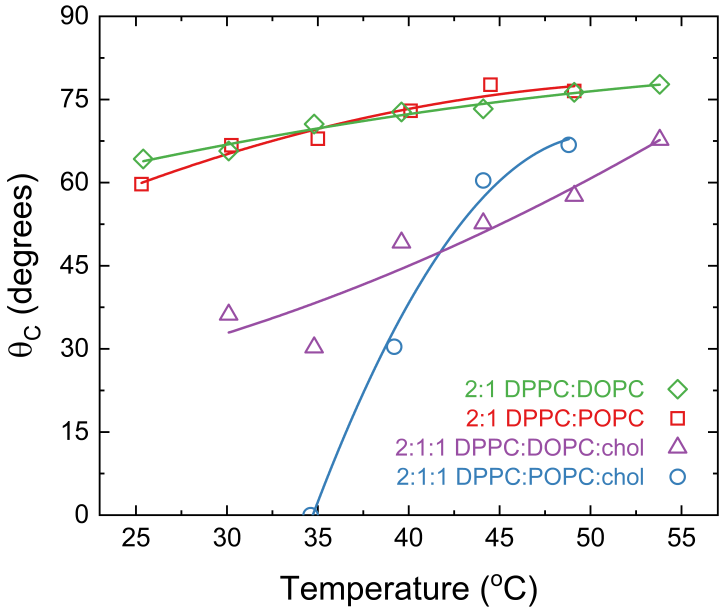

Figure 12: Temperature dependence of the half-cone angle for the Mu adducts of POPC in 2:1 DPPC:POPC and 2:1:1 DPPC:POPC:chol unilamellar vesicles and the Mu adducts of DOPC in 2:1 DPPC:DOPC and 2:1:1 DPPC:DOPC:chol unilamellar vesicles based on the $|\left\langle D_\mu^\parallel \right\rangle|$ values.

at 49 °C, while in 2:1 DPPC:DOPC it goes from 64° to 76° over the same temperature range. This would be within the error of the measurements. θ_C in the membranes containing chol is considerably smaller than in those without chol, which indicates that the motion of the acyl chains is significantly reduced in the presence of chol. The model breaks down in 2:1:1 DPPC:POPC:chol at lower temperatures as $|\left\langle D_\mu^\parallel \right\rangle|$ becomes larger than $D_\mu^\parallel$. This could be due to the DFT calculations not giving an accurate value of the dipolar coupling, but we also believe that at lower temperatures the rotation about the long axis of the chain is not rapid enough to average the dipolar coupling.

The full width half maximum of the Δ_1 resonance (Γ_1) gives information about the on-resonance damping rate (λ) for the Mu adducts of POPC and DOPC, which is caused by motion in the membrane. λ is calculated from Γ_1 and $|\left\langle D_\mu^\parallel \right\rangle|$ in the case of Lorentzian-like resonances using the following

equation [19]:

$$\lambda = \pi\sqrt{(\gamma_\mu \Gamma_1)^2 - \frac{27}{64}\left\langle D_\mu^{\parallel}\right\rangle^2} \tag{10}$$

We expect λ to have the classic form:

$$\lambda = W_{ij}\frac{2\tau_c}{1+\omega_{ij}^2\tau_c^2} \tag{11}$$

where ω_{ij} is the energy difference in frequency between the crossing levels i and j, W_{ij} is the matrix element, and τ_c is the correlation time for the motion causing the damping. Based on the temperature dependence, the system is in the motional narrowing regime where $\omega_{ij}^2\tau_c^2 \ll 1$. Under these conditions $\lambda \approx 2W_{ij}\tau_c$. We are assuming that the motion is activated, i.e. $\tau_c = \tau_0 e^{E_a/k_\mathrm{B}T}$, where E_a is the activation energy, and k_B is the Boltzmann constant. Combining these gives:

$$\ln\lambda = \ln 2W_{ij}\tau_0 + \left(\frac{E_\mathrm{a}}{k_\mathrm{B}}\right)T^{-1} \tag{12}$$

λ is larger in the biomembranes with chol at 30 °C than those without chol, with the values indicating that the motional correlation time is ∼4.5 times larger (i.e. slower) than in the DPPC:POPC and DPPC:DOPC membranes. This is further evidence that chol slows down the dynamics of the acyl chains. A plot of $\ln(\lambda)$ versus inverse temperature (Figure 13) is linear for all samples with the slope giving E_a. The activation energy is larger in the membranes containing chol; 38(5) kJ/mol in 2:1:1 DPPC:POPC:chol and 31(4) kJ/mol in 2:1:1 DPPC:DOPC:chol versus 16(5) kJ/mol in 2:1 DPPC:POPC and 23(2) kJ/mol in 2:1 DPPC:DOPC. The motion that is causing the on-resonance damping is unknown.

4.3. Temperature Dependence of Cholesterol Dynamics

In the 73:27 DPPC:chol sample there is coexistence between the liquid-ordered (L_o) and liquid-disordered (L_α) phases above ∼40 °C [38]. Below this temperature the sample is completely in the L_o phase. The ALC-μSR spectra of 73:27 DPPC:chol consist of relatively narrow resonances, which we associate with the L_α phase, that are superimposed on a broad feature that we assign to be overlapping resonances due to muoniated spin probes in the L_o phase combined with shifts in the baseline. A Δ_0 resonance due to $H_{4\beta}$

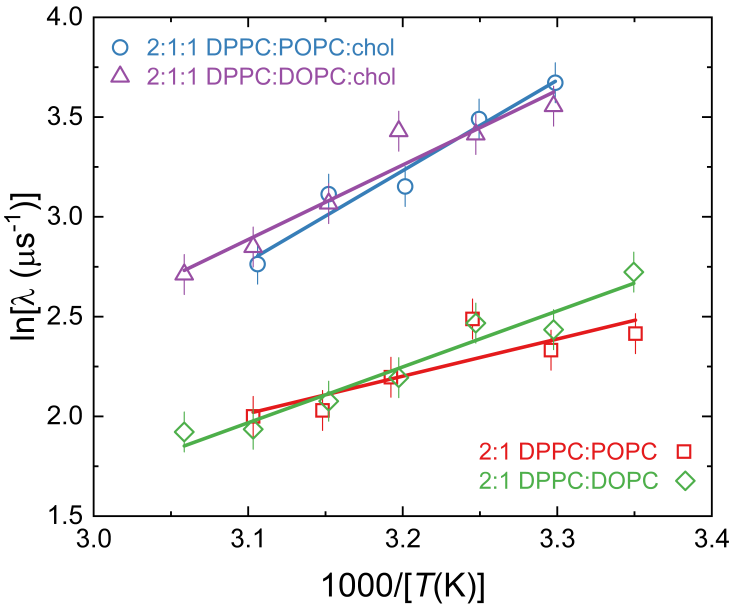

Figure 13: Arrhenius plot of the on-resonance relaxation rate versus inverse temperature for the Mu adducts of POPC in 2:1 DPPC:POPC and 2:1:1 DPPC:POPC:chol unilamellar vesicles and the Mu adducts of DOPC in 2:1 DPPC:DOPC and 2:1:1 DPPC:DOPC:chol unilamellar vesicles.

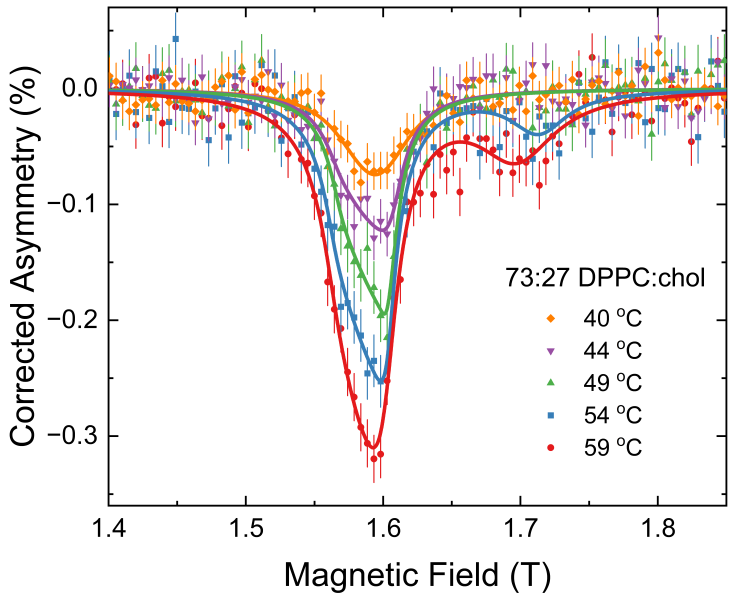

Figure 14: Background-subtracted ALC-μSR spectra of 73:27 DPPC:chol unilamellar vesicles as a function of temperature.

was observed at ∼1.7 T and above 54 °C. The Δ_1 resonance is much smaller and narrower in 73:27 DPPC:chol than in solid cholesterol [39] indicating substantially larger amplitude reorientational motion within the membrane. The amplitude of the Δ_1 resonance due to spin probes in the L_α phase increases with temperature and the resonance become increasingly asymmetric. The increase in the amplitude is due to the volume fraction of the L_α phase increasing with temperature. It is not observed below 40 °C due to the disappearance of the L_α phase. Conversely, the broad feature disappears with increasing temperature as the volume fraction of the L_o phase decreases and is difficult to disentangle from changes in the baseline. The ALC-μSR spectra are shown with the broad feature subtracted in order to focus on the resonances from spin probes in the L_α phase (Figure 14).

The Δ_1 resonance in 73:27 DPPC:chol is asymmetric so it was possible to determine $\left\langle D_\mu^\parallel \right\rangle$ directly using Eqs. 4 and 5. The values of $\left\langle D_\mu^\parallel \right\rangle$ as a function of temperature are shown in Figure 15. The Mu-6β-chol radical (and by inference chol) rotating rapidly about an axis corresponding to the smallest moment of inertia of the rigid steroid ring structure would result

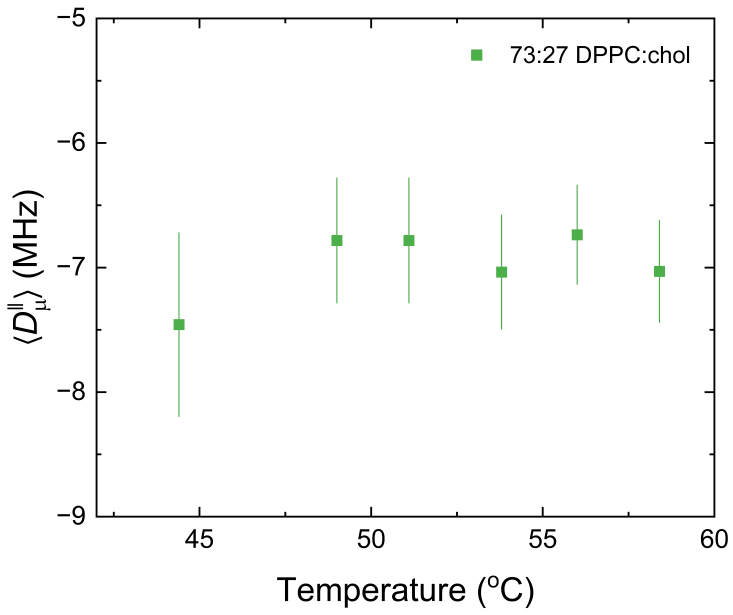

Figure 15: Temperature dependence of the motionally averaged dipolar muon hfcc of the Mu-6β-chol radical in 73:27 DPPC:chol unilamellar vesicles.

in $\left\langle D_\mu^\parallel \right\rangle$ = -4.2 MHz. This was obtained using Eq. 8 with values from DFT calculations at the ub3lyp/6-31g(d,p) level and with the C-Mu bond increased by a factor of 1.076 from the optimized value in order to mimic the light mass of the muon (Figure 16). The measured values have the same sign but are approximately 67% larger. This could be due to preferred rotation axis not corresponding exactly with the smallest moment of inertia of the rigid steroid ring structure. We can reproduce the measured values if the rotation axis is approximatly 7° from the x axis shown in Figure 16. The magnitude of $\left\langle D_\mu^\parallel \right\rangle$ does not change significantly with temperature in the L_α phase, which indicates that the orientation and the amplitude of the wobbling of chol about the preferred axis is roughly independent of temperature within the range studied.

The Δ_1 resonance of the Mu-6β-chol radical in 2:1:1 DPPC:POPC:chol is roughly Lorentzian shaped but unlike with the resonances due to the Mu adducts of POPC, it was not possible to determine $|\left\langle D_\mu^\parallel \right\rangle|$ as the Δ_0 resonance due to $H_{4\beta}$ was not observed. The Lorentzian lineshape of the Δ_1

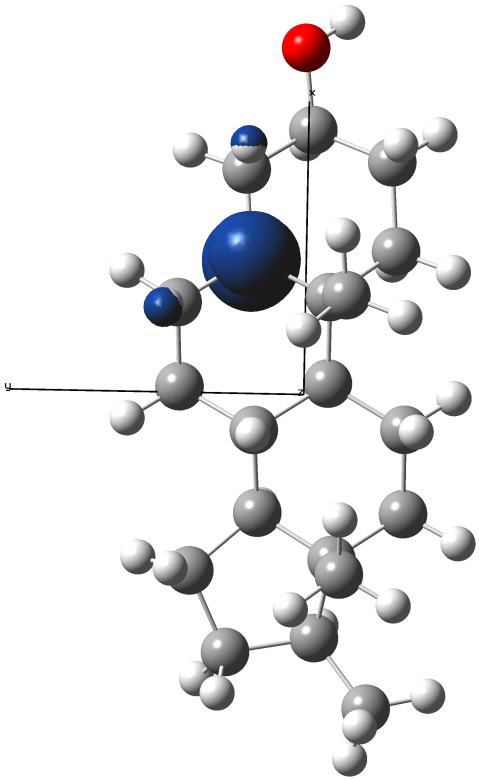

Figure 16: Structure of the Mu-6β-chol radical with a methyl group replacing the hydrocarbon tail at the ub3lyp/6-31g(d,p) level. Grey = carbon, white = hydrogen, red = oxygen. The blue surface is the spin density with a bounding value of 0.08. The vertical axis, corresponding to the smallest moment of inertia, was used to calculate $\left\langle D_{\mu}^{\parallel} \right\rangle$ = -4.2 MHz.

resonance in 2:1:1 DPPC:POPC:chol and that the resonance is narrower than in 73:27 DPPC:chol, suggests that $|\left\langle D_{\mu}^{\parallel} \right\rangle|$ is smaller when POPC is present, and consequently suggests chol is undergoing larger amplitude and faster motion. The unsaturated alkyl chain of POPC is increasing the area per molecule in the membrane, with the resulting greater space allowing for chol to move more freely in the membrane. This results in a less stiff or softer membrane.

5. Conclusions

ALC-μSR spectroscopy has been used to probe the nanoscale dynamics of in situ generated spin labels located in the acyl chain and on cholesterol in model phospholipid membranes. The presence of cholesterol significantly reduces the amplitude of restricted reorientational motion in the acyl chain at the C_9-C_{10} position and increases the torsional barrier for rotation about the bonds in the acyl chain. In other words, there is a stiffening of the unsaturated bilayer in the presence of chol. Swapping POPC for DOPC has very little effect on either the amplitude of restricted reorientational motion in the acyl chain or the torsional barrier.

References

[1] D. Marquardt, N. Kučerka, S. R. Wassall, T. A. Harroun, J. Katsaras, Cholesterol's location in lipid bilayers, Chemistry and Physics of Lipids 199 (2016) 17–25. doi:10.1016/j.chemphyslip.2016.04.001.

[2] S. Chakraborty, M. Doktorova, T. R. Molugu, F. A. Heberle, H. L. Scott, B. Dzikovski, M. Nagao, L.-R. Stingaciu, R. F. Standaert, F. N. Barrera, J. Katsaras, G. Khelashvili, M. F. Brown, R. Ashkar, How cholesterol stiffens unsaturated lipid membranes, Proceedings of the National Academy of Sciences 117 (36) (2020) 21896–21905. doi:10.1073/pnas.2004807117.

[3] F. T. Doole, T. Kumarage, R. Ashkar, M. F. Brown, Cholesterol stiffening of lipid membranes, The Journal of Membrane Biology 255 (4–5) (2022) 385–405. doi:10.1007/s00232-022-00263-9.

[4] J. F. Nagle, E. A. Evans, P. Bassereau, T. Baumgart, S. Tristram-Nagle, R. Dimova, A needless but interesting controversy, Proceedings of the National Academy of Sciences 118 (20) (May 2021). doi:10.1073/pnas.2025011118.

[5] J. Katsaras, T. Gutberlet, Lipid Bilayers, Springer Berlin Heidelberg, 2001. doi:10.1007/978-3-662-04496-4.

[6] M. Nagao, H. Seto, Neutron scattering studies on dynamics of lipid membranes, Biophysics Reviews 4 (2) (May 2023). doi:10.1063/5.0144544.

[7] T. R. Molugu, S. Lee, M. F. Brown, Concepts and methods of solid-state NMR spectroscopy applied to biomembranes, Chemical Reviews 117 (19) (2017) 12087–12132. doi:10.1021/acs.chemrev.6b00619.

[8] D. Marsh, Spin-Label Electron Paramagnetic Resonance Spectroscopy, CRC Press, 2019. doi:10.1201/9780429194634.

[9] D. G. Fleming, I. McKenzie, P. W. Percival, Muon Spin Spectroscopy: Methods and Applications in Chemistry and Materials, Wiley-VCH GmbH, 2024.

[10] S. L. Veatch, S. S. W. Leung, R. E. W. Hancock, J. L. Thewalt, Fluorescent probes alter miscibility phase boundaries in ternary vesicles, The Journal of Physical Chemistry B 111 (3) (2007) 502–504. doi:10.1021/jp067636i.

[11] N. J. Clayden, U. A. Jayasooriya, S. P. Cottrell, Dynamics of dioleoyl phosphatidylcholine by muon spin relaxation, Physical Chemistry Chemical Physics 1 (18) (1999) 4379–4382. doi:10.1039/a905031k.

[12] S. A. Barker, S. P. Cottrell, S. R. Giblin, U. A. Jayasooriya, Preliminary μSR studies on the incorporation of steroidal drug molecules into liposomes, Physica B: Condensed Matter 374–375 (2006) 332–335. doi:10.1016/j.physb.2005.11.089.

[13] H. L. Scott, A. Skinkle, E. G. Kelley, M. N. Waxham, I. Levental, F. A. Heberle, On the mechanism of bilayer separation by extrusion, or why your LUVs are not really unilamellar, Biophysical Journal 117 (8) (2019) 1381–1386. doi:10.1016/j.bpj.2019.09.006.

[14] I. McKenzie, R. Scheuermann, I. Tucker, Partitioning of 2-phenylethanol and limonene cosurfactants in $C_{12}E_4$, Physical Chemistry Chemical Physics 19 (14) (2017) 9551–9557. doi:10.1039/c7cp00668c.

[15] M. J. Frisch, G. W. Trucks, H. B. Schlegel, G. E. Scuseria, M. A. Robb, J. R. Cheeseman, G. Scalmani, V. Barone, B. Mennucci, G. A. Petersson, H. Nakatsuji, M. Caricato, X. Li, H. P. Hratchian, A. F. Izmaylov, J. Bloino, G. Zheng, J. L. Sonnenberg, M. Hada, M. Ehara, K. Toyota, R. Fukuda, J. Hasegawa, M. Ishida, T. Nakajima, Y. Honda, O. Kitao, H. Nakai, T. Vreven, J. A. Montgomery, Jr., J. E. Peralta, F. Ogliaro, M. Bearpark, J. J. Heyd, E. Brothers, K. N. Kudin, V. N. Staroverov, R. Kobayashi, J. Normand, K. Raghavachari, A. Rendell, J. C. Burant, S. S. Iyengar, J. Tomasi, M. Cossi, N. Rega, J. M. Millam, M. Klene, J. E. Knox, J. B. Cross, V. Bakken, C. Adamo, J. Jaramillo, R. Gomperts, R. E. Stratmann, O. Yazyev, A. J. Austin, R. Cammi, C. Pomelli, J. W. Ochterski, R. L. Martin, K. Morokuma, V. G. Zakrzewski, G. A. Voth, P. Salvador, J. J. Dannenberg, S. Dapprich, A. D. Daniels, O. Farkas, J. B. Foresman, J. V. Ortiz, J. Cioslowski, D. J. Fox, Gaussian 09 Revision E.1, gaussian Inc. Wallingford CT (2009).

[16] M. C. Böhm, R. Ramírez, J. Schulte, Finite-temperature properties of the muonium substituted ethyl radical CH_2MuCH_2: nuclear degrees of freedom and hyperfine splitting constants, Molecular Physics 103 (17) (2005) 2407–2436. doi:10.1080/00268970500159323.

[17] J. Israelachvili, J. Sjösten, L. Eriksson, M. Ehrström, A. Gräslund, A. Ehrenberg, ESR spectral analysis of the molecular motion of spin labels in lipid bilayers and membranes based on a model in terms of two angular motional parameters and rotational correlation times, Biochimica et Biophysica Acta (BBA) - Biomembranes 382 (2) (1975) 125–141. doi:10.1016/0005-2736(75)90171-6.

[18] E. Roduner, I. D. Reid, M. Riccò, R. D. Renzi, Anisotropy of 2-norbornyl radical reorientational dynamics in the plastic phase of norbornene as determined by ALC-μSR, Berichte der Bunsengesellschaft für physikalische Chemie 93 (11) (1989) 1194–1197. doi:10.1002/bbpc.19890931109.

[19] I. McKenzie, V. L. Karner, R. Scheuermann, Analysis of avoided level crossing muon spin resonance spectra of muoniated radicals in

anisotropic environments: Estimation of muon dipolar hyperfine parameters for lorentzian-like δ_1 resonances, Quantum Beam Science 8 (2) (2024) 15. doi:10.3390/qubs8020015.

[20] J. A. Weil, J. R. Bolton, Electron Paramagnetic Resonance: Elementary Theory and Practical Applications, Wiley, 2006. doi:10.1002/0470084987.

[21] D. G. Fleming, M. D. Bridges, D. J. Arseneau, Y. K. Chen, Y. A. Wang, Isotope effects and the temperature dependences of the hyperfine coupling constants of muoniated sec-butyl radicals in condensed phases, The Journal of Physical Chemistry A 115 (13) (2011) 2778–2793. doi:10.1021/jp109676b.

[22] I. McKenzie, R. Scheuermann, K. Sedlak, A. Stoykov, Molecular dynamics in rod-like liquid crystals probed by muon spin resonance spectroscopy, The Journal of Physical Chemistry B 115 (30) (2011) 9360–9368. doi:10.1021/jp203006w.

[23] J. Svetlovics, S. Wheaten, P. Almeida, Phase separation and fluctuations in mixtures of a saturated and an unsaturated phospholipid, Biophysical Journal 102 (11) (2012) 2526–2535. doi:10.1016/j.bpj.2012.04.017.

[24] G. Lindblom, G. Orädd, Lipid lateral diffusion and membrane heterogeneity, Biochimica et Biophysica Acta (BBA) - Biomembranes 1788 (1) (2009) 234–244. doi:10.1016/j.bbamem.2008.08.016.

[25] K. Simons, E. Ikonen, Functional rafts in cell membranes, Nature 387 (6633) (1997) 569–572. doi:10.1038/42408.

[26] D. Marsh, Cholesterol-induced fluid membrane domains: A compendium of lipid-raft ternary phase diagrams, Biochimica et Biophysica Acta (BBA) - Biomembranes 1788 (10) (2009) 2114–2123. doi:10.1016/j.bbamem.2009.08.004.

[27] J. Korlach, P. Schwille, W. W. Webb, G. W. Feigenson, Characterization of lipid bilayer phases by confocal microscopy and fluorescence correlation spectroscopy, Proceedings of the National Academy of Sciences 96 (15) (1999) 8461–8466. doi:10.1073/pnas.96.15.8461.

[28] H. Heerklotz, Triton promotes domain formation in lipid raft mixtures, Biophysical Journal 83 (5) (2002) 2693–2701. doi:10.1016/s0006-3495(02)75278-8.

[29] I. V. Polozov, K. Gawrisch, Characterization of the liquid-ordered state by proton MAS NMR, Biophysical Journal 90 (6) (2006) 2051–2061. doi:10.1529/biophysj.105.070441.

[30] C. Nicolini, P. Thiyagarajan, R. Winter, Small-scale composition fluctuations and microdomain formation in lipid raft models as revealed by small-angle neutron scattering, Physical Chemistry Chemical Physics 6 (24) (2004) 5531. doi:10.1039/b408928f.

[31] J. Pencer, T. Mills, V. Anghel, S. Krueger, R. M. Epand, J. Katsaras, Detection of submicron-sized raft-like domains in membranes by small-angle neutron scattering, The European Physical Journal E 18 (4) (2005) 447–458. doi:10.1140/epje/e2005-00046-5.

[32] L. Toppozini, S. Meinhardt, C. L. Armstrong, Z. Yamani, N. Kučerka, F. Schmid, M. C. Rheinstädter, Structure of cholesterol in lipid rafts, Physical Review Letters 113 (22) (2014) 228101. doi:10.1103/physrevlett.113.228101.

[33] D. Marquardt, F. A. Heberle, J. D. Nickels, G. Pabst, J. Katsaras, On scattered waves and lipid domains: detecting membrane rafts with x-rays and neutrons, Soft Matter 11 (2015) 9055–9072. doi:10.1039/C5SM01807B.

[34] D. Ahmadi, K. C. Thompson, V. García Sakai, R. Schweins, M. Moulin, M. Haertlein, G. A. Strohmeier, H. Pichler, V. T. Forsyth, D. J. Barlow, M. J. Lawrence, F. Foglia, Nanoscale structure and dynamics of model membrane lipid raft systems, studied by neutron scattering methods, Frontiers in Physics 10 (Apr. 2022). doi:10.3389/fphy.2022.864746.

[35] W. K. Subczynski, A. Wisniewska, J. S. Hyde, A. Kusumi, Three-dimensional dynamic structure of the liquid-ordered domain in lipid membranes as examined by pulse-EPR oxygen probing, Biophysical Journal 92 (5) (2007) 1573–1584. doi:10.1529/biophysj.106.097568.

[36] Y. K. Chen, D. G. Fleming, Y. A. Wang, Theoretical calculations of hyperfine coupling constants for muoniated butyl radicals,

The Journal of Physical Chemistry A 115 (13) (2011) 2765–2777. doi:10.1021/jp1096212.

[37] T. M. Ferreira, F. Coreta-Gomes, O. H. S. Ollila, M. J. Moreno, W. L. C. Vaz, D. Topgaard, Cholesterol and POPC segmental order parameters in lipid membranes: solid state ^{1}H-^{13}C NMR and MD simulation studies, Phys. Chem. Chem. Phys. 15 (6) (2013) 1976–1989. doi:10.1039/c2cp42738a.

[38] D. Marsh, Liquid-ordered phases induced by cholesterol: A compendium of binary phase diagrams, Biochimica et Biophysica Acta (BBA) - Biomembranes 1798 (3) (2010) 688–699. doi:10.1016/j.bbamem.2009.12.027.

[39] I. McKenzie, J. Cannon, D. Cordoni-Jordan, Characterization of muoniated spin probes in cholesterol by avoided level crossing muon spin resonance, Hyperfine Interactions 242 (1) (Oct. 2021). doi:10.1007/s10751-021-01740-8.